

A GENERAL SOLVER FOR THE PREDICTION OF FLUTTER AND BUFFET ONSET

David Quero¹, Christoph Kaiser¹, Jens Nitzsche¹

¹DLR (German Aerospace Center)
Bunsenstr  e 10, 37073, G  ttingen
David.QueroMartin@dlr.de

Keywords: Flutter, buffet, transonic flow, Loewner framework, aeroelastic derivatives, mode tracking

Abstract: A versatile solver capable of predicting both flutter and buffet onset, while considering structural feedback, is introduced. The methodology involves computing the (generalized) aerodynamic forces using a linear-frequency-domain (LFD) solver based on linearized unsteady Reynolds-averaged Navier-Stokes equations (URANS) with an appropriate turbulence closure model. A state-space model of the aerodynamic forces is generated through interpolation of the frequency-domain samples, which is the basis of the p - L method. Eigenvalues corresponding to fluid modes may be directly determined, eliminating the need for a priori pole selection as required by traditional rational function approximation techniques. Consequently, the pre-buffet frequency is accurately represented by the imaginary part of the fluid mode's eigenvalue. With this representation of the fluid modes, a flutter solver is derived, which is able to predict both classical flutter and buffet onset values. The solver is applied to the supercritical OAT15A airfoil in the pre-buffet region, verifying its capability to predict both flutter and buffet onset values.

1 INTRODUCTION

Modern aircraft cruise at transonic Mach numbers due to the high flight efficiency in this regime. Complex flow phenomena arise in this regime, leading to transonic aeroelastic phenomena with distinct characteristics. Among these, flutter and transonic buffet are of significant importance. Flutter is related to an aeroelastic instability typically caused by the coupling of two or more structural modes under the action of the induced unsteady aerodynamic forces, resulting in positive damping in the aeroelastic mode. Certification specifications, as outlined in the paragraph CS25.629 [1], require that aircraft be free of flutter in an extended flight envelope. This is defined by a 15 percent increase in equivalent airspeed at constant Mach number and constant altitude, covering all combinations of altitudes and speeds encompassed by the dive conditions (VD/MD) versus altitude. Transonic (or shock) buffet is related to a Hopf bifurcation by which a steady-state stable flow transitions into a self-sustained periodic solution at specific combinations of Mach number and angle of attack values. It results from the interaction between a shock wave and a boundary layer resulting in a shock motion.

The unsteadiness imposed by transonic buffet on the aircraft structure limits the flight envelope and fatigue life. For a civil aircraft, a certain margin must be reserved between the cruise state and the buffet onset boundary, which is computed neglecting the effect of the dynamic aircraft deformation on the flow itself. Operational regulations [2] dictate that the buffet onset should be

determined based on the normal acceleration experienced at the pilot station during flight tests. Typically, a vibration value of $\pm 0.05 g$ (with g the gravitational acceleration) has been used, although the appropriate acceleration level may vary depending on the aircraft and the dynamic response of the accelerometer. Additionally, a margin of $0.3 g$ to the buffet onset boundary is recommended to ensure maneuver capability during flight. Accurately predicting buffet onset is thus crucial for the design process. However, current industrial practice often relies on steady RANS analysis with the $\Delta\alpha = 0.1$ offset method. This method involves offsetting the linear portion of the lift curve against angle of attack α by 0.1 (deg). The intersection of this offset line with the actual lift curve is used to estimate buffet onset [3]. Unfortunately, this approach neglects the flow unsteadiness and its interaction with the flexible structure, known to play a key role in the determining buffet onset.

Previous work has considered the mutual interaction between a flexible structure and shock buffet. It has been shown, particularly for a pitch-plunge (and variants thereof) typical section aerofoil, that the introduction of an elastic structure has the ability to change the stability of an otherwise stable flow [4]. Gao et al. [5] also observed this phenomenon of reduction of the flutter onset by considering the heave or pitch degree-of-freedom (dof) separately. The consideration of the fluid mode by previous studies [4–10] has provided a new perspective on understanding transonic aeroelastic phenomena. Even though flutter and buffet onset must fulfill different margin conditions as specified by regulations, this new perspective allows for the computation of both phenomena within a unified framework. Due to the decreased flow stability in the transonic regime, the pole representing the dominant fluid mode plays a fundamental role to the fluid-structure interaction equation, resulting in different instability patterns as well as different aeroelastic phenomena. The dimensionless frequency ratio between the structural mode and the fluid mode is a key parameter affecting the characteristics of the coupled system. Furthermore, it has been shown that the frequency lock-in phenomenon is caused by the fluid mode rather than by a resonance mechanism [7].

Nitzsche et al. [4] highlighted the importance of considering structural feedback in predicting buffet onset. Houtman and Timme [10] obtained the shock buffet under the influence of a flexible structure using global stability analysis. Because the Schur complement method is unsuited for finding fluid instabilities due to the mathematical structure of the coupled physics, a full eigenvalue solution for the coupled aeroelastic system was considered. In this work, the extension of the p - L flutter solution method [11, 12] to include fluid modes is developed.

Two main methods for computing an aeroelastic instability onset can be used when considering the interplay effects between the dominant fluid mode and the structural ones, each with its own limitations:

- Nonlinear solvers: This approach involves using methods like the p - k [4, 13] and g [14] method to determine the eigensolutions to the flutter equation by solving a nonlinear algebraic equation. These methods may miss flutter instabilities that result from the coupling of fluid and structural modes if an appropriate initial solution for the aeroelastic modes is not provided. This limitation is discussed further in Section 3.
- Computation of aeroelastic eigensolutions: Two different methods can be applied here, namely, 1) the derivation of a state-space model for the aerodynamic system of much smaller size than the original high-fidelity problem, or 2) the use of tailored eigenvalue solvers for the full-size coupled aeroelastic problem. For the first method, the state-space representation of the aerodynamic system of smaller size are based either on time-domain

methods, such as DMD [4, 8] or autoregressive with exogenous input (ARX) model [5] or on frequency-domain methods, with a subsequent conversion into the time-domain required, as done in the p method [15–17] and the p - L method [11]. However, there is currently no automatic way to detect the aeroelastic mode related to the dominant fluid mode for these techniques. Either the “least-stable” fluid mode or a time-domain solution to compute the buffet frequency are required. Nevertheless, as discussed in Section 3.1, the “least-stable” fluid mode resulting from a state-space representation of the unsteady flow may not always be the most dominant one. For the second method, determining the eigenvalues corresponding to fluid modes typically requires a search. For each angle of attack, several shifts are distributed along the imaginary axis, along with a few shifts with positive growth rate, enabling a wider search radius albeit with a reduced convergence rate of the shift-and-invert spectral transformation.

To address the mentioned limitations, the development of more advanced methods becomes necessary for computing the buffet onset while considering the interplay between aerodynamic and structural forces. This necessity has been highlighted by Nitzsche et al. [4] and Houtman and Timme [10]. This work focuses on the describing aeroelastic instabilities in the transonic regime in the pre-buffet area and thus corresponding to the instability types I and II according to Gao and Zhang [8]. To achieve this, an eigenvalue solver able to determine the flutter and buffet onsets of instability without the need of generating time-domain data for the aerodynamic model is derived. Additionally, it automatically detects the dominant fluid mode responsible for the buffet onset, including the associated buffet frequency. This is accomplished by extending the p - L flutter solution method presented in Quero et al. [11] with an additional sweep prior to the classical flutter sweep. This new feature is complemented with a mode-tracking algorithm which is applicable to both the structural and fluid modes constituting the aeroelastic coupled system.

2 AEROELASTIC SOLVER FOR FLUTTER AND BUFFET ONSET PREDICTION

2.1 Rational representation of the aerodynamic term

In this work, aerodynamic data is assumed to be available in the frequency domain, specifically over the imaginary axis of the complex plane. The focus is on the transonic regime, requiring an appropriate model description, such as that obtained from the linearized URANS equations and implemented in the linear-frequency-domain (LFD) solver of the DLR computational fluid dynamics (CFD) TAU code [18]. Several techniques exist to transform the corresponding aerodynamic term in the frequency domain into a suitable generalized state-space form in the time domain. Most of these techniques require providing the aerodynamic poles’ locations [19–21], or if not, they rely on a nonlinear optimization method [22, 23]. Typically, aerodynamic stable poles distributed along the negative real axis are chosen for methods requiring their manual selection [19–21]. However, including complex aerodynamic poles is essential in the transonic regime, as the imaginary part of the most dominant fluid mode represents the buffet frequency. Other methods, such as the autoregressive model with exogenous input (ARX) [5] or the eigen-system realization algorithm (ERA) [24], can also provide complex aerodynamic poles with a non-zero imaginary part. However, they require the generation of input-output data in the time domain, while in this work the efficient LFD solver in the frequency domain is preferred.

The Loewner framework [11, 25] generates the required (generalized) state-space model by interpolating the provided aerodynamic term in the frequency domain. For further details, the techniques for obtaining the aerodynamic generalized state-space model are described in Quero

et al. [11] and are not repeated here. When used for aeroservoelastic applications in the time domain, the model generated with the Loewner framework requires an additional stabilization procedure [26,27], as the derived model may include unstable poles. The stabilization technique used in this work, although optional when searching for aeroelastic eigensolutions, is presented in Section 2.1.1.

2.1.1 Residualization and stabilization procedure

For the purpose of this work of detecting flutter and buffet onset, stabilization enforcement is not required, provided that an appropriate mode-tracking algorithm, such as that of Section 2.3, is used. However, to enable simulation of the resulting model in the time domain, a stabilization procedure is employed. This is justified in the pre-buffet region where the fluid modes are still stable. Note that beyond the Hopf bifurcation, a stable limit-cycle oscillation occurs, and time-domain simulations must consider nonlinear terms in the aerodynamic model. Possible stabilization procedures are described in [26, 27]. In this work, a stabilization procedure that provides results similar to those provided of the RH_∞ projection, is easy to apply, and converts the generalized state-space matrices corresponding to a descriptor system into a regular state-space model, is chosen. The method is described next.

Upon application of the Loewner framework [11] to the generalized aerodynamic forces (GAF) matrix at a particular Mach number M_∞ and a steady condition defined by the angle of attack α_0 , the matrices $\mathbf{E}_{a0}(\alpha_0, M_\infty) \in \mathbb{R}^{n_a \times n_a}$, $\mathbf{A}_{a0}(\alpha_0, M_\infty) \in \mathbb{R}^{n_a \times n_a}$, $\mathbf{B}_{a0}(\alpha_0, M_\infty) \in \mathbb{R}^{n_a \times n_h}$ and $\mathbf{C}_{a0}(\alpha_0, M_\infty) \in \mathbb{R}^{n_h \times n_a}$ are obtained. These represent a generalized state-space model that interpolates the GAF matrix over the imaginary axis, that is, in the frequency domain. A transformation to obtain real entries in these matrices has already been applied [11]. The set of eigenvalues $\lambda(\mathbf{E}_{a0}, \mathbf{A}_{a0})$ such that $\det(\lambda \mathbf{E}_{a0} - \mathbf{A}_{a0}) = 0$ is computed numerically. For clarity, the explicit dependence of the matrices on (α_0, M_∞) has been omitted. From the computed eigenvalues, a subset with eigenvalues below a defined numerical tolerance λ_∞ is retained: $\lambda_f = \{\lambda \in \lambda(\mathbf{E}_{a0}, \mathbf{A}_{a0}) \mid |\lambda| \leq \lambda_\infty\}$. Additionally, if unstable eigenvalues are present, they are retained by mirroring them through the imaginary axis by exchanging the sign of their real part:

$$\lambda_a = \{\lambda \in \lambda_f \mid \text{Re}\{\lambda\} \leq 0\} \cup \{-\text{Re}\{\lambda\} + i\text{Im}\{\lambda\} \mid \lambda \in \lambda_f \text{ and } \text{Re}\{\lambda\} > 0\}.$$

With the total number n_{a0} of kept stable aerodynamic poles within the tolerance λ_∞ , a least-squares fit to the GAF matrix $\mathbf{Q}_{hh}(\alpha_0, M_\infty, ik)$ is imposed in the frequency domain:

$$\sum_{m=1}^{n_r} \frac{\mathbf{R}_{r,m}(\alpha_0, M_\infty)}{ik - \lambda_{r,m}} + \sum_{n=1}^{n_c} \left[\frac{\mathbf{R}_{c,n}(\alpha_0, M_\infty)}{ik - \lambda_{c,n}} + \frac{\bar{\mathbf{R}}_{c,n}(\alpha_0, M_\infty)}{ik - \bar{\lambda}_{c,n}} \right] + \mathbf{Q}_0(\alpha_0, M_\infty) + \mathbf{Q}_1(\alpha_0, M_\infty) ik - \mathbf{Q}_2(\alpha_0, M_\infty) k^2 = \mathbf{Q}_{hh}(\alpha_0, M_\infty, ik), \quad (1)$$

where n_r is the number of real aerodynamic poles $\lambda_{a,m}$ satisfying $\text{Im}\{\lambda_{a,m}\} = 0$ and n_c is the number of complex conjugate pairs of poles such that $n_{a0} = n_r + 2n_c$. The symbol $\bar{\cdot}$ denotes the complex conjugate and the matrices $\mathbf{R}_{r,m}(\alpha_0, M_\infty) \in \mathbb{C}^{n_h \times n_h}$ ($\mathbf{R}_{c,n}(\alpha_0, M_\infty)$ and $\bar{\mathbf{R}}_{c,n}(\alpha_0, M_\infty)$) are the residues associated to the eigenvalue or pole $\lambda_{r,m}$ ($\lambda_{c,n}$ and $\bar{\lambda}_{c,n}$). Due to the realness of the generalized state-space matrices, the residues and poles, if complex, appear in conjugate pairs. The polynomial term up to second order in the reduced frequency addresses the behavior at infinity, so that no matrix \mathbf{E}_a is further required. The least-squares fit from Eq. 1 is carried out for each element of the GAF matrix $\mathbf{Q}_{hh}(\alpha_0, M_\infty, ik)$ sharing the same set of aerodynamic poles $\lambda_a = \{\lambda_{r,1}, \dots, \lambda_{r,n_r}, \lambda_{c,1}, \bar{\lambda}_{c,1}, \dots, \lambda_{c,n_c}, \bar{\lambda}_{c,n_c}\}$.

Upon solving the least-squares procedure defined in Eq. 1, the resulting associated state-space matrices corresponding to the computed residue-pole form must be obtained. This is done via rank factorization [28] of the residue matrix $\mathbf{R}_{r,m} = \mathbf{U}_m \boldsymbol{\Sigma}_m \mathbf{V}_m^*$ for the real eigenvalues, which can be computed by applying a singular-value decomposition (SVD) and extracting the rank r_m with a numerical tolerance from the singular values in the diagonal of the matrix $\boldsymbol{\Sigma}_m$. This means that a number of r_m singular values above a numerical tolerance σ_0/σ_1 , with σ_1 the first entry in the diagonal matrix of the SVD decomposition, are kept. The tolerance σ_0 is set to $\sigma_0 = 10^{-6}$. The resulting state-space submatrices (where, for clarity, the dependence on (α_0, M_∞) has been omitted) for a real pole are:

$$\begin{aligned} \mathbf{A}_{r,m} &= \lambda_{r,m} \mathbf{I}_{r_m} \in \mathbb{C}^{r_m \times r_m}, \quad \mathbf{B}_{r,m} = (\mathbf{T}_m^T \boldsymbol{\Sigma}_m \mathbf{T}_m) (\mathbf{V}_m \mathbf{T}_m)^* \in \mathbb{C}^{r_m \times n_h}, \\ \mathbf{C}_{r,m} &= \mathbf{U}_m \mathbf{T}_m \in \mathbb{C}^{n_h \times r_m}, \quad m = 1, \dots, n_r, \end{aligned} \quad (2)$$

where \mathbf{I}_{r_m} is the identity matrix of size r_m and the matrix $\mathbf{T}_m \in \mathbb{R}^{n_h \times r_m}$ extracts the first r_m columns.

For a complex conjugate pair, the SVD decompositions are denoted as $\mathbf{R}_n = \mathbf{U}_n \boldsymbol{\Sigma}_n \mathbf{V}_n^*$ and $\bar{\mathbf{R}}_n = \bar{\mathbf{U}}_n \boldsymbol{\Sigma}_n \mathbf{V}_n^T$, so that the corresponding state-space submatrices are:

$$\begin{aligned} \mathbf{A}_{c,n} &= \begin{bmatrix} \lambda_n \mathbf{I}_{r_n} & \mathbf{0} \\ \mathbf{0} & \bar{\lambda}_n \mathbf{I}_{r_n} \end{bmatrix} \in \mathbb{C}^{2r_n \times 2r_n}, \quad \mathbf{B}_{c,n} = \begin{bmatrix} (\mathbf{T}_n^T \boldsymbol{\Sigma}_n \mathbf{T}_n) (\mathbf{V}_n \mathbf{T}_n)^* \\ (\mathbf{T}_n^T \boldsymbol{\Sigma}_n \mathbf{T}_n) (\mathbf{V}_n^T \mathbf{T}_n) \end{bmatrix} \in \mathbb{C}^{2r_n \times n_h}, \\ \mathbf{C}_{c,n} &= [\mathbf{U}_n \mathbf{T}_n \quad \bar{\mathbf{U}}_n \mathbf{T}_n] \in \mathbb{C}^{n_h \times 2r_n}, \quad n = 1, \dots, n_c, \end{aligned} \quad (3)$$

where r_n represents the rank of the matrix $\boldsymbol{\Sigma}_n$. Finally, the state-space matrices are obtained by concatenating the matrices provided in Eqs. 2 and 3 [28]:

$$\begin{aligned} \mathbf{A}_{ac} &= \begin{bmatrix} \mathbf{A}_{r,1} & \mathbf{0} & \cdots & & \mathbf{0} \\ \mathbf{0} & \ddots & & & \vdots \\ \vdots & & \mathbf{A}_{r,n_r} & & \\ & & & \mathbf{A}_{c,1} & \\ \mathbf{0} & \cdots & & \ddots & \mathbf{0} \\ & & & \mathbf{0} & \mathbf{A}_{c,n_c} \end{bmatrix}, \\ \mathbf{B}_{ac} &= \begin{bmatrix} \mathbf{B}_{r,1} \\ \vdots \\ \mathbf{B}_{r,n_r} \\ \mathbf{B}_{c,1} \\ \vdots \\ \mathbf{B}_{c,n_c} \end{bmatrix}, \quad \mathbf{C}_{ac} = [\mathbf{C}_{r,1} \quad \cdots \quad \mathbf{C}_{r,n_r} \quad \mathbf{C}_{c,1} \quad \cdots \quad \mathbf{C}_{c,n_c}]. \end{aligned}$$

Lastly, the obtained state-space matrices are converted to ensure that only real entries are present:

$$\mathbf{A}_{a1} = \mathbf{T} \mathbf{A}_{ac} \mathbf{T}^*, \quad \mathbf{B}_{a1} = \mathbf{T} \mathbf{B}_{ac}, \quad \mathbf{C}_{a1} = \mathbf{C}_{ac} \mathbf{T}^*,$$

where the matrix \mathbf{T} converts the complex state-space matrices to real:

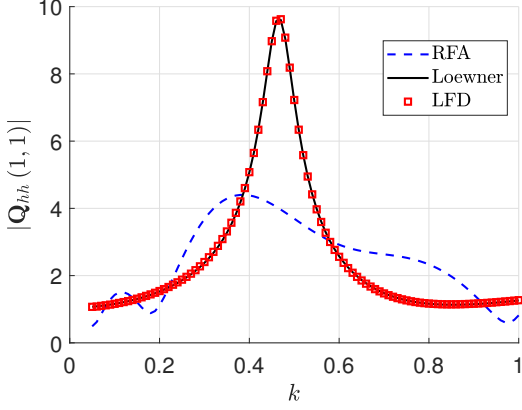


Figure 1: Absolute value of the pitch/pitch component of the GAF matrix \mathbf{Q}_{hh} against reduced frequency. Mach number is 0.73 and angle of attack 4 (deg).

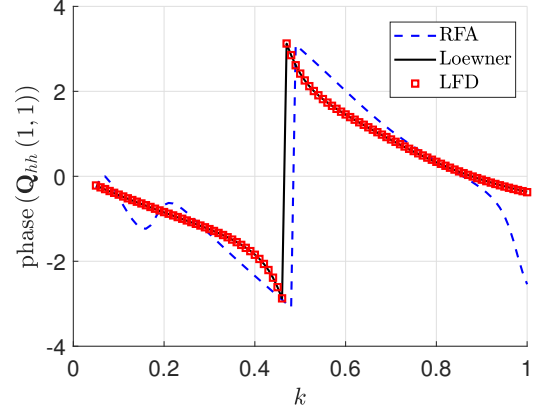


Figure 2: Phase of the pitch/pitch component of the GAF matrix \mathbf{Q}_{hh} against reduced frequency. Mach number is 0.73 and angle of attack 4 (deg).

$$\mathbf{T} = \begin{bmatrix} \mathbf{I}_{n_{ar}} & \mathbf{0} \\ \mathbf{0} & \mathbf{I}_{n_{ac}} \otimes \mathbf{J} \end{bmatrix}, \quad \mathbf{J} = \frac{1}{\sqrt{2}} \begin{bmatrix} 1 & 1 \\ -i & i \end{bmatrix},$$

with $n_{ar} = \sum_{m=1}^{n_r} r_m$ and $n_{ac} = 2 \sum_{n=1}^{n_c} r_n$ so that $n_a = n_{ar} + n_{ac} \leq n_{a0}$, where n_a is the resulting number of aerodynamic states required for the interpolation of the GAF matrix $\mathbf{Q}_{hh}(\alpha_0, M_\infty, ik)$. If a reduction in the total number of aerodynamic states n_a is desired, a balanced truncation can be applied to the state-space matrices $\mathbf{A}_{a1}(\alpha_0, M_\infty)$, $\mathbf{B}_{a1}(\alpha_0, M_\infty)$ and $\mathbf{C}_{a1}(\alpha_0, M_\infty)$ [29].

2.1.2 Importance of complex aerodynamic poles

To emphasize the importance of complex aerodynamic poles in accurately representing the GAF matrix in transonic flow, a comparison of the realization obtained by the classical Roger's RFA [19] using 8 poles distributed over the negative real axis according to [19], and the Loewner framework is shown in Figs. 1 (absolute value) and 2 (phase). For a fair comparison, the resulting model obtained with the Loewner framework was reduced to a total of 8 states, and the stabilization procedure of Section 2.1.1 was applied. The test case corresponds to the OAT15A airfoil at Mach number 0.73, an angle of attack 4 (deg), and Reynolds number 3 million, as in Section 3. The pitch rotation axis is located at 40 % of the airfoil chord measured from the leading edge. The pitch/pitch component of the GAF matrix $\mathbf{Q}_{hh}(\alpha_0, M_\infty, ik)$ is depicted (note that the explicit dependence of the GAF matrix on the Reynolds number has been omitted, as it considered constant).

The realization obtained with the classical Roger's RFA fails to represent the peak associated with the stamp left by the complex aerodynamic pole over the imaginary axis at the buffet frequency. No improvement was achieved by increasing the number of real poles, as the least-squares fit became numerically ill-conditioned. In contrast, the generalized state-space obtained using the Loewner and shifted-Loewner matrices accurately captures the reference data in the frequency domain, as obtained by the LFD solver.

Fig. 3 shows the eigenvalues from the state-space realizations corresponding to the RFA approximation and the Loewner framework. The Loewner framework is used as the basis for the

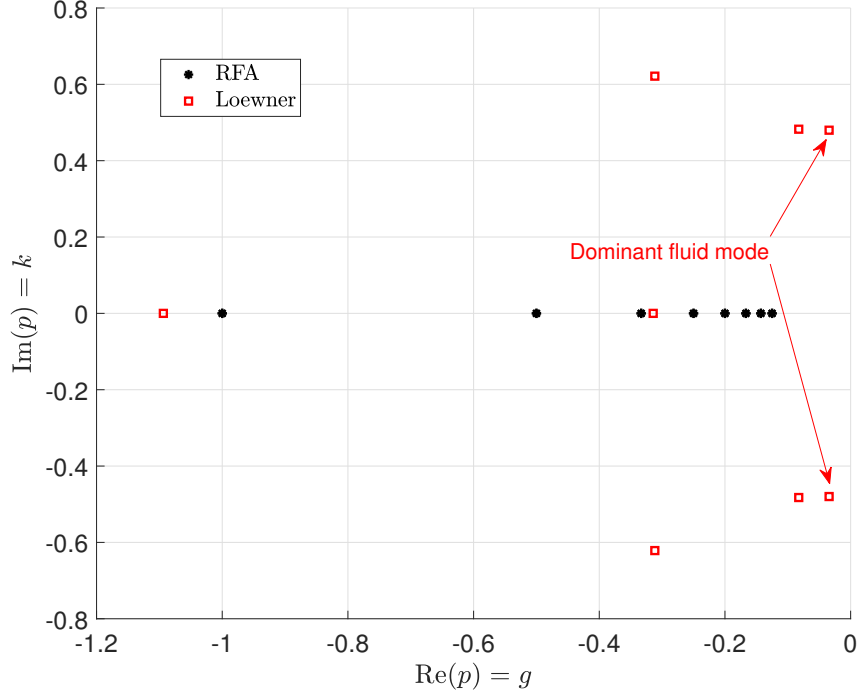


Figure 3: Aerodynamic poles corresponding to the RFA approximation and the Loewner realization in the non-dimensional complex plane. Mach number is 0.73 and angle of attack ranges 4 (deg).

p - L flutter solution method and is denoted as such in the figure. Each realization considers 8 aerodynamic poles. Unlike the RFA case, where the aerodynamic poles are manually chosen to lie on the negative real axis, the poles for the Loewner framework are not user-selected but are instead determined by the realization process. As will be shown in Section 3.1, the imaginary part of the dominant fluid mode, with a value of 0.4798, corresponds to the pre-buffet reduced frequency and is automatically detected by the realization carried out using the Loewner framework. The dominant fluid mode for the Loewner realization has been extracted according to the method described in Section 2.3 and in this case corresponds to the one closest to the imaginary axis or “least-stable” pole, but this is not always the case (see Section 3.1).

Once the suitability of the chosen approach has been verified, the aerodynamic state-space model is coupled with the structural model in Section 2.2, and the problem for determining aeroelastic instabilities (flutter and buffet onset) is formulated in Section 2.3.

2.2 Coupling with the structural model and general formulation

Once the aerodynamic and structural dynamic models are coupled, the number of n_g dof describing the structural behavior is reduced after applying a modal truncation, retaining a number n_h of representative natural eigenmodes of the structure in the matrix $\phi_0 \in \mathbb{R}^{n_g \times n_h}$. These modes are obtained as eigenvectors of the structure (wind-off conditions) with no damping. The resulting aeroelastic system in the Laplace domain is represented by the following flutter equation:

$$\left[p^2 \left(\frac{U_\infty}{L_{ref}} \right)^2 \mathbf{M}_{hh} + p \left(\frac{U_\infty}{L_{ref}} \right) \mathbf{B}_{hh} + \mathbf{K}_{hh} - q_{dyn} \mathbf{Q}_{hh}(p, M_\infty) \right] \mathbf{u}_h(p) = \mathbf{0}, \quad (4)$$

where $p = sL_{ref}/U_\infty = g + ik$ is obtained by nondimensionalizing the complex Laplace variable s , with L_{ref} a reference length and U_∞ the freestream airspeed. The matrices \mathbf{M}_{hh} ,

\mathbf{B}_{hh} and \mathbf{K}_{hh} represent the generalized mass, damping and stiffness, respectively. The p - L flutter solution method reformulates the aerodynamic forces caused by the motion, described by the set of n_n generalized coordinates \mathbf{u}_h , resulting in the following equation in generalized state-space form [11]:

$$\begin{aligned} & \begin{bmatrix} \mathbf{I} & \mathbf{0} & \mathbf{0} \\ \mathbf{0} & \mathbf{I} & \mathbf{0} \\ \mathbf{0} & \mathbf{0} & \mathbf{E}_a(\alpha_0, M_\infty) \end{bmatrix} \frac{d}{dt} \left(\begin{bmatrix} \mathbf{u}_h \\ \frac{d\mathbf{u}_h}{dt} \\ \mathbf{x}_a \end{bmatrix} \right) \\ &= \begin{bmatrix} \mathbf{0} & \mathbf{I} & \mathbf{0} \\ \alpha_{hh}^{-1}(rq_{dyn}\mathbf{Q}_0 - \mathbf{K}_{hh}) & \alpha_{hh}^{-1}(rq_{dyn}\mathbf{Q}_1 - \mathbf{B}_{hh}) & \alpha_{hh}^{-1}q_{dyn} \left(\frac{U_\infty}{L_{ref}} \right) \mathbf{C}_a(\alpha_0, M_\infty) \\ \mathbf{B}_a(\alpha_0, M_\infty) & \mathbf{0} & \left(\frac{U_\infty}{L_{ref}} \right) \mathbf{A}_a(\alpha_0, M_\infty) \end{bmatrix} \begin{bmatrix} \mathbf{u}_h \\ \frac{d\mathbf{u}_h}{dt} \\ \mathbf{x}_a \end{bmatrix}, \end{aligned} \quad (5)$$

where $\alpha_{hh} = \mathbf{M}_{hh} - rq_{dyn}\mathbf{Q}_2$ and:

$$\mathbf{A}_a(\alpha_0, M_\infty) = r\mathbf{A}_{a1}(\alpha_0, M_\infty) + (1-r)\mathbf{A}_{a0}(\alpha_0, M_\infty), \quad (6)$$

$$\mathbf{E}_a(\alpha_0, M_\infty) = r\mathbf{I}_{n_a} + (1-r)\mathbf{E}_{a0}(\alpha_0, M_\infty), \quad (7)$$

and similarly for $\mathbf{B}_a(\alpha_0, M_\infty)$ and $\mathbf{C}_a(\alpha_0, M_\infty)$. The factor (U_∞/L_{ref}) accounts for the conversion from the reduced frequency, where the realization of the GAF matrix has been carried out, to the circular frequency ω . The parameter $r = \{0, 1\}$ in Eq. 5 indicates whether the residualization procedure of Section 2.1.1 has been applied ($r = 1$) or not ($r = 0$). In Eq. 5 $q_{dyn} = \rho_\infty U_\infty^2/2$ denotes the dynamic pressure, with ρ_∞ the freestream density. The reduced frequency corresponds to the imaginary part of the complex Laplace variable p , defined as $k = \text{Im}\{p\} = \omega L_{ref}/U_\infty$, where ω denotes the circular frequency. In a more compact notation:

$$\mathbf{E}_{ae}(\alpha_0, M_\infty) \frac{d\mathbf{x}_{ae}}{dt} = \mathbf{A}_{ae}(\alpha_0, M_\infty, q_{dyn}) \mathbf{x}_{ae},$$

where $\mathbf{E}_{ae}(\alpha_0, M_\infty) \in \mathbb{R}^{(2n_h+n_a) \times (2n_h+n_a)}$, $\mathbf{A}_{ae}(\alpha_0, M_\infty, q_{dyn}) \in \mathbb{R}^{(2n_h+n_a) \times (2n_h+n_a)}$ and $\mathbf{x}_{ae} = \left[\mathbf{u}_h^T \left(\frac{d\mathbf{u}_h}{dt} \right)^T \mathbf{x}_a^T \right]^T \in \mathbb{R}^{2n_h+n_a}$. The stability of the aeroelastic system can now be analyzed by solving a generalized eigenvalue problem with generalized eigenvalue λ and generalized eigenvector ϕ :

$$(\lambda \mathbf{E}_{ae}(\alpha_0, M_\infty) - \mathbf{A}_{ae}(\alpha_0, M_\infty, q_{dyn})) \phi = \mathbf{0}, \quad (8)$$

Unlike flutter solvers such as the p - k and g methods, which rely on the solution of a nonlinear algebraic equation and require an initial guess for the aeroelastic eigensolution, Eq. 8 provides all eigenvalues of the aeroelastic system. This forms the basis of the p - L flutter solution method, provided the aerodynamic term has been obtained using of the Loewner and shifted-Loewner matrices. Note that if the relevant fluid mode is included along with the structural modes in Eq. 8, its solution provides the flutter (if the instability is caused by one or more structural modes) and buffet instability (if the instability is caused by one or more fluid modes) onset values, where the buffet onset computation will include the effect of the structural feedback on the unsteady aerodynamics.

2.3 Extended mode-tracking procedure including fluid and structural modes

Once the generalized eigenvalue problem has been formulated in Eq. 8, a technique to track the aeroelastic eigensolution as a parameter β changes is sought. Different choices for the parameter β can be considered, such as the freestream velocity U_∞ , the freestream density ρ_∞ , or the atmospheric altitude h [12]. The following description follows that provided in Quero et al. [12] for using aeroelastic sensitivities to track the aeroelastic modes.

Assume that the solution defined by the linear generalized eigenvalue problem of Eq. 8 at a stage j , defined by a particular value of the parameter β , is known. For the next value of the parameter β at the stage $j + 1$ associated with an increase in the dynamic pressure q_{dyn} , a first-order Taylor approximation may be applied provided the change in the aeroelastic eigensolution is *small*:

$$\tilde{\lambda}^{(j+1)} = \lambda^{(j)} + \left(\frac{d\lambda}{d\beta} \right)^{(j)} \Delta\beta, \quad \tilde{\phi}^{(j+1)} = \phi^{(j)} + \left(\frac{d\phi}{d\beta} \right)^{(j)} \Delta\beta \quad (9)$$

Thus, each eigensolution at the next parameter value $\beta^{(j+1)} = \beta^{(j)} + \Delta\beta$ may be estimated once the derivative terms $(d\lambda/d\beta)^{(j)}$ and $(d\phi/d\beta)^{(j)}$ are known. In order to obtain them, Eq. 8 is derived with respect to the parameter β :

$$\left(\mathbf{A}_{ae} - \lambda^{(j)} \mathbf{E}_{ae} \right) \left(\frac{d\phi}{d\beta} \right)^{(j)} + \left(\frac{d\mathbf{A}_{ae}}{d\beta} - \left(\frac{d\lambda}{d\beta} \right)^{(j)} \mathbf{E}_{ae} - \lambda^{(j)} \frac{d\mathbf{E}_{ae}}{d\beta} \right) \phi^{(j)} = \mathbf{0}. \quad (10)$$

Noticing that the generalized aeroelastic eigensolution obtained by Eq. 8 does not result in unique eigenvectors (only their direction is determined), an additional constraint is introduced with help of the weighting matrix \mathbf{W} ,

$$\left(\phi^{(j)} \right)^T \mathbf{W} \phi^{(j)} = W_0. \quad (11)$$

Choosing a matrix \mathbf{W} which is real and symmetric, a linear system of complex equations for the determination of the aeroelastic derivatives $(d\lambda/d\beta)^{(j)}$ and $(d\phi/d\beta)^{(j)}$ can be obtained:

$$\begin{bmatrix} -\mathbf{E}_{ae} \phi^{(j)} & \mathbf{A}_{ae} - \lambda^{(j)} \mathbf{E}_{ae} \\ \mathbf{0} & 2 \left(\phi^{(j)} \right)^T \mathbf{W} \end{bmatrix} \begin{bmatrix} \left(\frac{d\lambda}{d\beta} \right)^{(j)} \\ \left(\frac{d\phi}{d\beta} \right)^{(j)} \end{bmatrix} = \begin{bmatrix} - \left(\frac{d\mathbf{A}_{ae}}{d\beta} - \lambda^{(j)} \frac{d\mathbf{E}_{ae}}{d\beta} \right) \phi^{(j)} \\ - \left(\phi^{(j)} \right)^T \frac{d\mathbf{W}}{d\beta} \phi^{(j)} \end{bmatrix}. \quad (12)$$

Note that the use of the additional constraint given by Eq. 11 requires the scaling of the eigenvectors obtained after solving the linear generalized eigenvalue defined by Eq. 8. In this work, the matrix \mathbf{W} is chosen to be the identity, $\mathbf{W} = \mathbf{I}_{2n_h+n_a}$. With this choice, the term $d\mathbf{W}/d\beta$ in the right-hand side of Eq. 12 is identically a zero matrix, $d\mathbf{W}/d\beta = \mathbf{0}$. Additionally, the constant W_0 is set to 1 in Eq. 11, $W_0 = 1$, so that the aeroelastic eigenvector $\phi^{(j)}$ is scaled as:

$$\phi^{(j)} = \frac{\phi_0^{(j)}}{\sqrt{\left(\phi_0^{(j)} \right)^T \mathbf{W} \phi_0^{(j)}}},$$

with $\phi_0^{(j)} \in \mathbb{C}^{2n_h+n_a}$ the unscaled eigenvector obtained by direct solution of Eq. 8 and $\mathbf{W} = \mathbf{I}_{2n_h+n_a}$. Aeroelastic derivatives $d\mathbf{A}_{ae}/d\beta$ and $d\mathbf{E}_{ae}/d\beta$ required for the right-hand side term of Eq. 12 are provided in [12] for different scenarios for the case $r = 0$. For the application cases of Section 3, a residualization has been used ($r = 1$), and thus the derivatives are computed numerically by finite differences.

After determining the aeroelastic eigensolution by solving Eq. 8, the first-order approximation of the eigensolution provided by Eq. 9 is used (with the derivatives provided by Eq. 12) together with a scalar which combines information from both the eigenvalue and eigenvector [12, 30]. The aeroelastic modes are then assigned by choosing the one corresponding to the smallest scalar value.

Note that the classical flutter solution process includes the aeroelastic modes corresponding to the structural modes in wind-off conditions. In this work, the aim is to augment those modes by automatically including the dominant fluid mode in the analysis so that the buffet onset value can be computed within the same solver, namely, by the eigenvalue solution provided in Eq. 8. This is carried out in a two-step process, as described next.

Step 1

To select the dominant fluid modes, the pure aerodynamic system without structural feedback is considered first. These are obtained by computing the eigenvalues $\lambda(\mathbf{E}_a, \mathbf{A}_a)$, where the (generalized) state-space matrices are provided in Eqs. 7 and 6 respectively. Recall that $r = 1$ if the residualization of Section 2.1.1 is applied; otherwise $r = 0$.

To assess the significance of the aerodynamic poles within the GAF matrix over the imaginary axis, the residues \mathbf{R}_j associated with each aerodynamic pole $\lambda_{a,j}$ are computed. These residues are determined using the generalized two-sided Rayleigh quotient:

$$\mathbf{R}_j = \frac{(\mathbf{C}_a \phi_j) (\psi_j^* \mathbf{B}_a)}{\psi_j^* \mathbf{E}_a \phi_j}, \quad j = 1, \dots, n_a,$$

where ϕ_j and ψ_j are the right and left eigenvectors associated to the eigenvalue $\lambda_{a,j}$, that is, $\mathbf{A}_a \phi_j = \lambda_{a,j} \mathbf{E}_a \phi_j$ and $\psi_j^* \mathbf{A}_a = \lambda_{a,j} \psi_j^* \mathbf{E}_a$. The Rayleigh quotient, a fundamental tool in the dominant pole algorithm (DPA) [31–33], is used here. However, given the comparatively low number of states n_a required to represent the GAF matrix in relation to the actual number of flow states required in the CFD model, in this work the Rayleigh quotient is computed for each of the aerodynamic poles individually, obviating the need for iterative DPA application. Once the residue of the aerodynamic poles \mathbf{R}_j are available, the following criterion is employed to evaluate the significance of each pole contribution to the GAF matrix:

$$\delta_j = \|\mathbf{R}_j\|_2 / \text{Re} \{ \lambda_{a,j} \}, \quad j = 1, \dots, n_{ar} + n_{ac}/2, \quad (13)$$

where $\|\cdot\|_2$ represents the 2-norm of the residue matrix \mathbf{R}_j . As complex aerodynamic poles occur in conjugate pairs, only the set of aerodynamic poles satisfying $\text{Im} \{ \lambda_{a,j} \} \geq 0$ is considered when evaluating δ_j with Eq. 13. From the total of $n_{ar} + n_{ac}/2$ available poles, n_d dominant aerodynamic poles, as specified by the user, are then chosen such that $\delta_1 \geq \delta_2 \geq \dots \geq \delta_{n_d}$.

After extracting the n_d dominant fluid modes, the aeroelastic system in its p - L formulation as given in Eq. 5, accounting for coupling effects between the aerodynamic and structural models, is considered. To recreate conditions where the aerodynamic system remains unaffected by structural terms, a factor q_m premultiplying the matrix $\alpha_{hh} = \mathbf{M}_{hh} - r q_{dyn} \mathbf{Q}_2$, that is, $q_m \alpha_{hh}$, is introduced in Eq. 5. Alternatively, only the mass matrix \mathbf{M}_{hh} may be multiplied by the factor q_m . By letting $q_m \rightarrow \infty$ the pure aerodynamic problem without structural effects is restored, as the second block-row in the matrix $\mathbf{A}_{ae}(\alpha_0, M_\infty, q_{dyn})$ approaches zero and the eigenvalues $\lambda(\mathbf{E}_a(\alpha_0, M_\infty), \mathbf{A}_a(\alpha_0, M_\infty))$ become a subset of the eigenvalues provided by Eq. 8. Additional (almost) zero eigenvalues λ corresponding to the structural dof are obtained when solving Eq. 8 and can be disregarded.

By assigning the closest eigenvalues obtained from Eq. 8 to the previously obtained dominant fluid modes through evaluation of the criterion defined in Eq. 13, the dominant fluid modes can be subsequently tracked while setting the aeroelastic parameter $\beta = q_m$, with its value progressively decreased from $q_m \rightarrow \infty$ to $q_m = 1$, whereby the dynamic pressure is fixed to the desired value $q_{dyn,0}$. This is typically a small value, say $q_{dyn,0} = 0.1$ (Pa), thus representing the common flutter sweep starting from a low dynamic pressure value. Both the structural and dominant fluid modes are now encompassed in the analysis and can be tracked while increasing the dynamic pressure, as described in step 2 below.

Step 2

In step 2, the classical sweep is conducted, where the dynamic pressure is increased from the initial value $q_{dyn,0}$, kept constant during step 1, to the desired level. Throughout this process, the value $q_m = 1$ remains constant, as the variation in q_m was solely required to incorporate additional dominant fluid modes at the beginning of step 2. The aeroelastic parameter β is set to U_∞ , ρ_∞ , or the flight altitude h . If the dynamic pressure in step 1 ($q_{dyn,0}$) was set to a small value representing a wind-off condition, the structural modes can be assigned to a subset of the aeroelastic modes obtained by solving Eq. 8. As previously noted, the most dominant fluid mode is already identified from step 1 and can be seamlessly included in this sweep. By subsequently increasing the aeroelastic parameter β , the evolution of both the structural and most dominant fluid modes with increasing dynamic pressure value can be effectively tracked.

3 APPLICATION CASE

In this section the methods of Section 2 are applied to an aeroelastic system consisting of an OAT15A supercritical airfoil [34] and a two dof structural model including heave and pitch motions. For the structural model, the pitch rotation axis is located at 40 % of the airfoil chord, and the structural matrices are defined as follows:

$$\mathbf{M}_{hh} = \begin{bmatrix} 48.1056 \text{ (kg)} & 0 \\ 0 & 4.8106 \text{ (kg m}^2\text{)} \end{bmatrix}, \quad \mathbf{K}_{hh} = \begin{bmatrix} 2.5322 \cdot 10^5 \text{ (N/m)} & 0 \\ 0 & 0.4502 \cdot 10^5 \text{ (N m)} \end{bmatrix},$$

whereas the structural damping has been set to zero. The corresponding natural frequencies are 11.547 (Hz) and 15.396 (Hz) for the heave and pitch dof, respectively.

Regarding for the aerodynamic model, Fig. 4 depicts the unstructured mesh used for the URANS modeling employing the Spalart-Allmaras (SA) turbulence closure model, as detailed by Nitzsche et al. [4]. The Mach number is 0.73, the Reynolds number 3 million and the freestream temperature 273.15 (K).

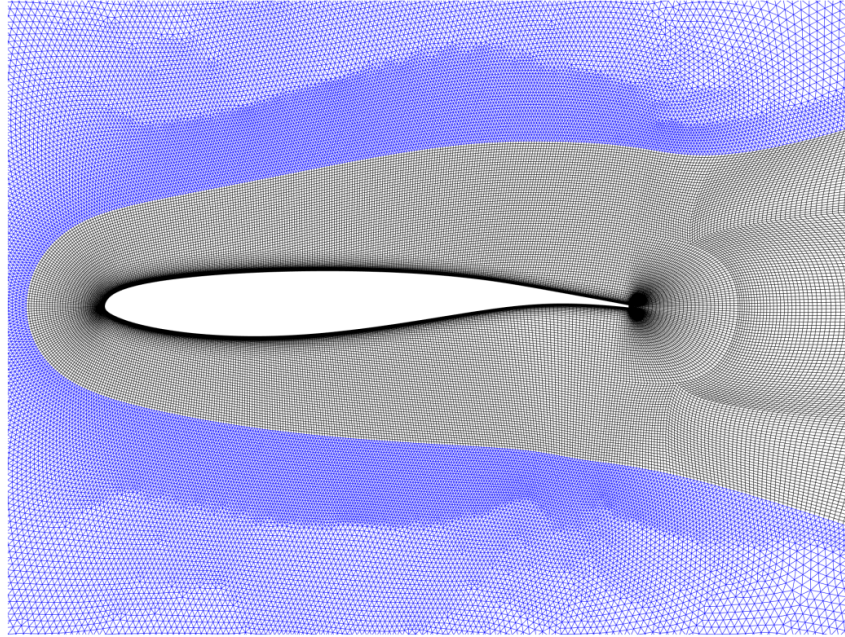


Figure 4: OAT15A airfoil mesh, Mach number 0.73, Reynolds number 3 million and freestream temperature 273.15 (K) [4].

3.1 Fluid modes extraction

Prior to the computation of buffet and flutter onset values at different conditions, the adequacy of the p - L method to describe the dominant fluid mode is investigated. To that aim the pure aerodynamic system, that is, without structural feedback, is considered. This corresponds to the initial stage of Step 1 in Section 2.3, where the dominant fluid modes are extracted. Fig. 5 depicts the location of a subset of 100 fluid modes as extracted directly from the DLR-CFD TAU model together with the most dominant fluid mode obtained using the p - L method in conjunction with the criterion given in Eq. 13. The directly extracted fluid modes are found as the eigenvalues of the spatially discretized flux Jacobian matrix of the DLR-CFD TAU model [35]. Evaluated at the steady-state flow solution and normalized by the cell volumes, this matrix describes the linear, time-invariant dynamics of the flow. A subset of eigenvalues in a specified region of the matrix's spectrum is computed by employing the implicitly restarted Arnoldi method [36] in combination with the shift-and-invert method.

The positive imaginary part of the complex plane is shown, as the fluid modes appear in complex conjugate pairs. Note the relative agreement between both methods and the correct trend regarding the increase in angle of attack. However, slight differences exist between the methods and further comparison with the eigenvalues extracted from the linearized CFD solver shall be focus of future research. It is worth noting that fluid modes closer to the imaginary axis are obtained from the linearized CFD solver compared to those representing buffet onset in Fig. 5, particularly evident in cases where the angle of attack is 3 or 6 (deg). This highlights the fact that the criterion for dominance of a fluid mode involves not only the distance to the imaginary axis but also the residue value, as addressed in Eq. 13. Consequently, the terms “least-stable” or “dominant” fluid mode, as mentioned in [6], should not be used interchangeably, and the term “most dominant” fluid mode is proposed.

When applying the p - L method to represent the GAF matrix, two observations made by Gao et al. [6] can be confirmed:

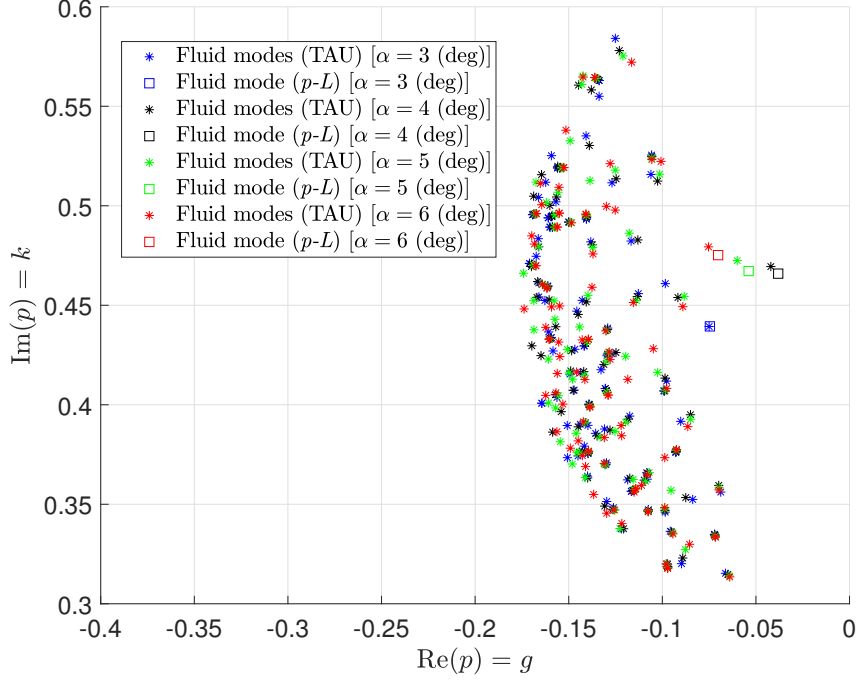


Figure 5: Fluid modes obtained with the DLR-TAU CFD solver and the p - L method. Mach number is 0.73 and angle of attack ranges from 3 to 6 (deg) in 1 (deg) increment.

- The dominant fluid mode remains unaffected by the generalized coordinates representing structural motion. This has been verified by modifying the pitch axis of rotation of the airfoil, yielding nearly identical values for the aerodynamic poles corresponding to the dominant fluid mode. This observation also aligns with the peak identified by Nitzsche [37] in the aerodynamic frequency response, which remains consistent regardless of the motion imposed on the airfoil contour. This peak represents the stamp left by the dominant fluid mode on the imaginary axis, with its imaginary part representing the buffet frequency.
- The selection of order for the realization of the GAF matrix within the p - L method can influence the fluid modes, except for the dominant one. This implies that while the contribution of the dominant fluid mode to the aerodynamic transfer function matrix (GAF) is paramount, adjustments to the location and residue values of other fluid modes lead to similar contributions to the GAF matrix.

3.2 Aeroelastic instabilities in the pre-buffet region

In this section the stability of the aeroelastic system for two different steady angle of attack α_0 values is considered. For these two different values, the predicted instabilities are attributed to different aeroelastic modes. When $\alpha_0 = 0$, a classical flutter-type instability is identified, whereby the aeroelastic mode causing the instability can be traced back to an structural mode when the dynamic pressure is reduced. Conversely, for $\alpha_0 = 4$ (deg) the observed arises from the fluid mode under structural feedback, corresponding the reduction of flutter onset case [4,5].

To verify the predicted instabilities, a classical flutter solver type based on the solution of the nonlinear algebraic equation presented in Eq. 4 is considered. The g method [14] has been chosen as the classical flutter solver, as no solutions could be found for the $\alpha_0 = 4$ (deg) case using the p - k method [13] when tracking the fluid mode.

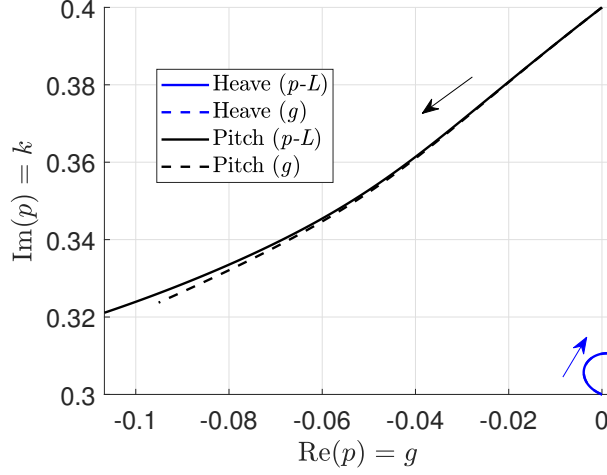


Figure 6: Aeroelastic modes corresponding to the structural modes (sweep in density). Mach number is 0.73 and angle of attack 0 (deg).

Angle of attack $\alpha_0 = 0$

In this case classical flutter is observed for the combination of parameters considered. Thus, the evolution of the aeroelastic modes corresponding to the structural modes for wind-off conditions when increasing the dynamic pressure is depicted in Fig. 6, where the arrows point out the direction of the increasing parameter β , which is taken to be the density ρ . The density is increased from a very small value of 10^{-8} (kg/m³) up to 0.3 (kg/m³) with an increment value of $\Delta\beta = \Delta\rho = 0.002$ (kg/m³). The condition at which the aeroelastic mode corresponding mainly to the heave motion crosses the imaginary axis indicates the flutter onset. Both the p - L method and the classical g method predict the same values. The corresponding density at the flutter onset condition is $\rho_F = 0.24$ (kg/m³) and the aeroelastic mode frequency $f_F = 11.95$ (Hz), with a corresponding reduced flutter reduced frequency $k_F = 0.31$. For increasing values of the real part, the predictions for the aeroelastic modes deviate between the two methods, as the g method progressively loses its validity for increasing distances from the imaginary axis, while the p - L method retains its prediction capabilities [11].

The dominant fluid mode is not depicted because no buffet onset is observed. The flutter onset value has been obtained considering the two structural dof. If a similar flutter onset instability were observed considering only one structural dof, this would correspond to the type I instability as defined by Gao and Zhang [8].

Angle of attack $\alpha_0 = 4$ (deg)

In this case a buffet onset value is predicted for increasing density values. The results corresponding to steps 1 and 2, as described in Section 2.3, are presented. Fig. 7 shows the aeroelastic mode corresponding to the dominant fluid mode when decreasing the value q_m from 10^{12} down to $q_m = 1$. A variable step size Δq_m has been considered and the arrow points in the direction of decreasing q_m . The dynamic pressure is set to a constant value of $q_{dyn,0} = 0.001$ (Pa).

Once the dominant fluid mode has been tracked to $q_m = 1$, step 2 described in Section 2.3 is carried out. As for the $\alpha_0 = 0$ case, the parameter β is the density ρ . Its value is increased from that corresponding to the dynamic pressure $q_{dyn,0}$ up to a value of $\rho = 0.1046$ (kg/m³) in increments of $\Delta\beta = \Delta\rho = 0.002$ (kg/m³). Figs. 8 and 9 show the evolution of the aeroelastic and fluid modes during step 2, respectively, where the arrows indicate the direction of increasing density ρ . As previously stated, the fluid mode could not be found for any density value when

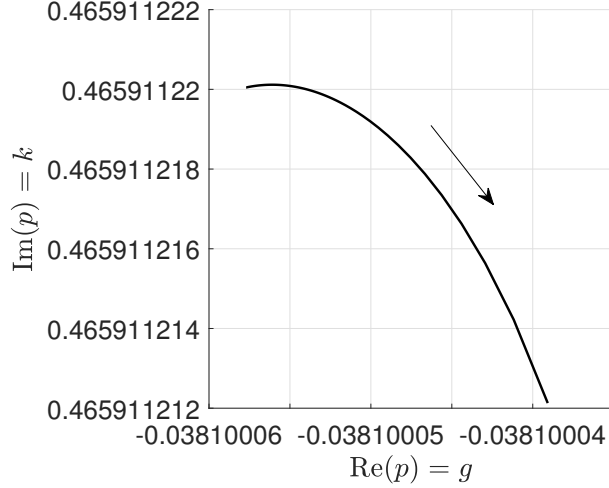


Figure 7: Fluid mode evolution in step 1 (sweep in q_m). Mach number is 0.73 and angle of attack 4 (deg).

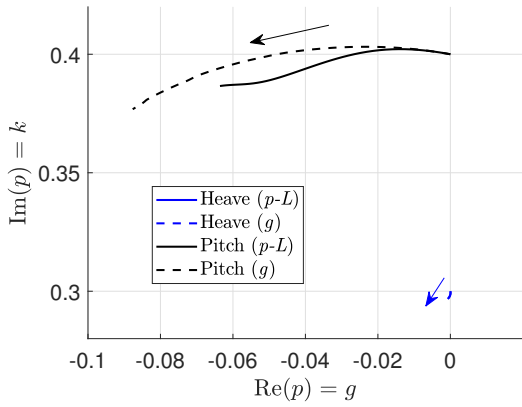


Figure 8: Aeroelastic modes corresponding to the structural modes (sweep in density). Mach number is 0.73 and angle of attack 4 (deg).

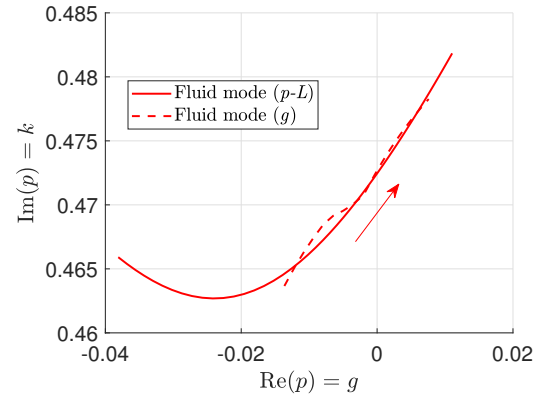


Figure 9: Aeroelastic modes corresponding to the dominant fluid mode (sweep in density). Mach number is 0.73 and angle of attack 4 (deg).

using the p - k flutter solution method. The g method was able to track the fluid mode for a limited range of density values in the interval $[0.0426 \ 0.0958]$ (kg/m^3), using the initial frequency value as provided by the buffet frequency of the dominant fluid mode. For density values outside this interval, the g method could not find the fluid mode. The buffet onset value occurs at a density value of $\rho_B = 0.067$ (kg/m^3) for a reduced frequency of $k_B = 0.47268$, very close to the pre-buffet frequency. This phenomenon corresponds to the type II instability as defined by Gao and Zhang [8], which is characterized by a reduction in the buffet onset due to structural feedback.

This example showcases the advantage of the proposed method, as it provides the buffet onset prediction in an automated manner, similar to the flutter onset prediction for the $\alpha_0 = 0$ case. In contrast, classical flutter solution methods based on the nonlinear solution of Eq. 4 were unable to find the aeroelastic mode representative of the dominant fluid mode, or if they did, it was limited to parameter interval after providing an initial value for the search, requiring prior knowledge of the system, such as the buffet frequency. This is not required by the proposed general flutter solver, as the dominant fluid mode is automatically included in the search and the buffet frequency is a result of the tracking procedure.

4 CONCLUSIONS

In this work, a general flutter solver based on the p - L method [11] is presented, capable of predicting both flutter and buffet onset values. The solver automatically computes instabilities caused by structural and fluid modes, providing the buffet frequency without requiring a user search, as global stability analysis methods do. The solver can incorporate multiple fluid modes, allowing for the application of different mode-tracking techniques. Specifically, the mode-tracking procedure by Quero et al. [12] has been extended to include fluid modes. Both residualized and non-residualized forms of the (generalized) aerodynamic state-space are considered. This involves computing aeroelastic sensitivities numerically, and using finite differences for their approximation has been shown to yield robust results.

The aerodynamic term is represented by a (generalized) state-space model, obtained by interpolating the frequency-domain data from high-fidelity CFD solvers. In this work, the LFD method is used. Unlike classical RFA techniques, this unsteady aerodynamic model includes aerodynamic poles with nonzero imaginary parts, essential for representing the pre-buffet frequency. A criterion is proposed to select the most dominant fluid mode from the generated unsteady aerodynamic model, demonstrating that the “least-stable” fluid mode and the dominant fluid mode are not necessarily equivalent. The pre-buffet frequency is extracted from the imaginary part of the dominant fluid mode, eliminating the need for a user search as required by global stability analysis methods.

Furthermore, it is shown that classical flutter solution methods, which solve a nonlinear eigenvalue problem, lack robustness when searching for the fluid mode. These methods fail to numerically find the aeroelastic mode corresponding to the dominant fluid mode, regardless of the initial values provided for the search. In contrast, the proposed method simultaneously identifies the aeroelastic modes corresponding to both the fluid and structural modes.

The eigenvalue corresponding to the dominant fluid mode has been verified against values obtained from global stability analysis at various angles of attack without structural feedback. Future work shall address this verification including structural feedback.

The application of the proposed method is not limited to the presented example. It can also address other phenomena where aeroelastic modes associated with fluid modes cross the imaginary axis. These include the vortex breakdown in delta wing configurations [38] or the consideration of multiple relevant fluid modes in pre-buffet regions for three-dimensional configurations [9]. Thus, future work shall explore applying this method to more complex configurations.

5 REFERENCES

- [1] European Aviation Safety Agency (EASA) (2007). Certification specifications for large aeroplanes CS-25. https://www.easa.europa.eu/sites/default/files/dfu/CS-25_Amdt%203_19.09.07_Consolidated%20version.pdf (accessed May 2024).
- [2] Federal Aviation Administration (FAA) (2018). Advisory circular, flight test guide for certification of transport category airplanes, chapter 10. https://www.faa.gov/documentLibrary/media/Advisory_Circular/AC_25-7D.pdf (accessed May 2024).

- [3] Kenway, G. and Martins, J. (2017). Buffet-onset constraint formulation for aerodynamic shape optimization. *AIAA Journal*, 55(6). <https://doi.org/10.2514/1.J055172>.
- [4] Nitzsche, J., Ringer, L., Kaiser, C., et al. (2019). Fluid-mode flutter in plane transonic flows. In *IFASD Conference Proceedings*. https://elib.dlr.de/188433/1/IFASD_2022_149.pdf (accessed May 2024).
- [5] Gao, C., Zhang, W., and Ye, Z. (2018). Reduction of transonic buffet onset for a wing with activated elasticity. *Aerospace Science and Technology*, 77, 670–676. <https://doi.org/10.1016/j.ast.2018.03.047>.
- [6] Gao, C., Zhang, W., and Ye, Z. (2016). A new viewpoint on the mechanism of transonic single-degree-of-freedom flutter. *Aerospace Science and Technology*, 103(103266). <https://doi.org/10.1016/j.ast.2016.02.029>.
- [7] Gao, C., Zhang, W., Li, X., et al. (2017). Mechanism of frequency lock-in in transonic buffeting flow. *Journal of Fluid Mechanics*, 818, 528–561. <https://doi.org/10.1017/jfm.2017.120>.
- [8] Gao, C. and Zhang, W. (2020). Transonic aeroelasticity: A new perspective from the fluid mode. *Progress in Aerospace Sciences*, 113(100596). <https://doi.org/10.1016/j.paerosci.2019.100596>.
- [9] Timme, S. (2020). Global instability of wing shock-buffet onset. *Journal of Fluid Mechanics*, 885. <https://doi.org/10.1017/jfm.2019.1001>.
- [10] Houtman, J. and Timme, S. (2021). Towards global stability analysis of flexible aircraft in edge-of-the-envelope flow. In *AIAA Scitech Forum*. Virtual Event. <https://doi.org/10.2514/6.2021-0610>.
- [11] Quero, D., Vuillemin, P., and Poussot-Vassal, C. (2021). A generalized eigenvalue solution to the flutter stability problem with true damping: The p - L method. *Journal of Fluids and Structures*, 103(103266). <https://doi.org/10.1016/j.jfluidstructs.2021.103266>.
- [12] Quero, D., Vuillemin, P., and Poussot-Vassal, C. (2022). Improved mode tracking for the p - L flutter solution method based on aeroelastic derivatives. In *IFASD Conference Proceedings*. <https://elib.dlr.de/187885/1/IFASD-2022-018.pdf> (accessed May 2024).
- [13] Hassig, H. (1971). An approximate true damping solution of the flutter equation by determinant iteration. *Journal of Aircraft*, 8(11), 885–889. <https://doi.org/10.2514/3.44311>.
- [14] Chen, P. (2000). Damping perturbation method for flutter solution: The g -method. *AIAA Journal*, 38(9), 1519–1524. <https://doi.org/10.2514/2.1171>.
- [15] Burkhart, T. (1977). Subsonic transient lifting surface aerodynamics. *Journal of Aircraft*, 14(1). <https://doi.org/10.2514/3.58748>.

- [16] Abel, I. (1979). An analytical technique for predicting the characteristics of a flexible wing equipped with an active flutter-suppression system and comparison with wind-tunnel data. *NASA Technical Paper 1367*. <https://ntrs.nasa.gov/api/citations/19790009093/downloads/19790009093.pdf> (accessed May 2024).
- [17] Rodden, W. and Bellinger, E. (1982). Aerodynamic lag functions, divergence, and the british flutter method. *Journal of Aircraft*, 19(7). <https://doi.org/10.2514/3.44772>.
- [18] Thormann, R. and Widhalm, M. (2013). Linear-frequency-domain predictions of dynamic-response data for viscous transonic flows. *AIAA journal*, 51(11), 2540–2557. <https://doi.org/10.2514/1.J051896>.
- [19] Roger, K. L. (1977). Airplane math modeling methods for active control design. *AGARD-CP-228*, 4.1–4.11.
- [20] Karpel, M. (1982). Design for active flutter suppression and gust alleviation using state-space aeroelastic modeling. *Journal of Aircraft*, 19(3), 221–227. <https://doi.org/10.2514/3.57379>.
- [21] Morino, L., Mastroddi, F., Troia, R. D., et al. (1995). Matrix fraction approach for finite-state aerodynamic modeling. *AIAA Journal*, 33(4), 703–711. <https://doi.org/10.2514/3.12381>.
- [22] Pasinetti, G. and Mantegazza, P. (1999). Single finite states modeling of aerodynamic forces related to structural motions and gusts. *AIAA Journal*, 37(5), 604–612. <https://doi.org/10.2514/2.760>.
- [23] Ripepi, M. and Mantegazza, P. (2013). Improved matrix fraction approximation of aerodynamic transfer matrices. *AIAA Journal*, 51(5), 1156–1173. <https://doi.org/10.2514/1.J052009>.
- [24] Juang, J. and Pappa, R. (1985). An eigensystem realization algorithm for modal parameter identification and model reduction. *Journal of Guidance, Control and Dynamics*, 8(5). <https://doi.org/10.2514/3.20031>.
- [25] Mayo, A. and Antoulas, A. (2007). A framework for the solution of the generalized realization problem. *Linear algebra and its applications*, 425(2-3), 634–662. <https://doi.org/10.1016/j.laa.2007.03.008>.
- [26] Quero, D., Vuillemin, P., and Poussot-Vassal, C. (2019). A generalized state-space aeroservoelastic model based on tangential interpolation. *Aerospace*, 6(1), 9. <https://doi.org/10.3390/aerospace6010009>.
- [27] Gosea, I., Zhang, Q., and Antoulas, A. (2020). Preserving the DAE structure in the Loewner model reduction and identification framework. *Advances in Computational Mathematics*, 46(1), 3. <https://doi.org/10.1007/s10444-020-09752-8>.
- [28] Gilbert, E. (1963). Controllability and observability in multivariable control systems. *Journal of the Society for Industrial and Applied Mathematics, Series A: Control*, 1(2), 128–151. <https://doi.org/10.1137/0301009>.

- [29] Moore, B. (1981). Principal component analysis in linear systems: Controllability, observability, and model reduction. *IEEE Transactions on Automatic Control*, 26(1), 17–32. <https://doi.org/10.1109/TAC.1981.1102568>.
- [30] Yue, C. and Zhao, Y. (2021). Interpolation-based modeling methodology for efficient aeroelastic control of a folding wing. *International Journal of Aerospace Engineering*, 2021. <https://doi.org/10.1155/2021/8609211>.
- [31] Martins, M. and Quintão, P. (2003). Computing dominant poles of power system multivariable transfer functions. *IEEE Transactions on Power Systems*, 18(1), 152–159. <https://doi.org/10.1109/TPWRS.2002.807040>.
- [32] Rommes, J. and Martins, N. (2006). Efficient computation of multivariable transfer function dominant poles using subspace acceleration. *IEEE Transactions on Power Systems*, 21(4), 1471–1483. <https://doi.org/10.1109/TPWRS.2006.881154>.
- [33] Sleijpen, G. and Rommes, J. (2008). Computing dominant poles of transfer functions. *High Performance Algorithms for Computational Science and Their Applications*, 1614, 111–123.
- [34] Deck, S. (2005). Numerical simulation of transonic buffet over a supercritical airfoil. *AIAA Journal*, 43(7). <https://doi.org/10.2514/1.9885>.
- [35] Dwight, R., Brezillon, J., and Vollmer, D. (Toulouse, France, 2006). Efficient algorithms for solution of the adjoint compressible Navier-Stokes equations with applications. *ONERA-DLR Aerospace Symposium (ODAS)*. <https://elib.dlr.de/50793/1/rdwight-odas2006-AdjointAlgorithms.pdf> (accessed May 2024).
- [36] Lehoucq, R. and Sorensen, D. (1996). Deflation techniques for an implicitly restarted Arnoldi iteration. *SIAM Journal on Matrix Analysis and Applications*, 17(4). <https://doi.org/10.1137/S089547989528148>.
- [37] Nitzsche, J. (2009). A numerical study on aerodynamic resonance in transonic separated flow. In *IFASD Conference Proceedings*. https://elib.dlr.de/61964/1/J._Nitzsche_-_A_NUMERICAL_STUDY_ON_AERODYNAMIC_RESONANCE.pdf (accessed May 2024).
- [38] Werner, M. (2023). Numerische untersuchung der wirbel-wirbel- und wirbel-stoß-interaktion in transsonischen strömungen. *Phd Thesis, Technische Hochschule Aachen*. <https://publications.rwth-aachen.de/record/959034/files/959034.pdf> (accessed May 2024).

COPYRIGHT STATEMENT

The authors confirm that they, and/or their company or organisation, hold copyright on all of the original material included in this paper. The authors also confirm that they have obtained permission from the copyright holder of any third-party material included in this paper to publish it as part of their paper. The authors confirm that they give permission, or have obtained permission from the copyright holder of this paper, for the publication and public distribution of this paper as part of the IFASD 2024 proceedings or as individual off-prints from the proceedings.